

Dipolar Hole-Blocking Layers for Inverted Perovskite Solar Cells: Effects of Aggregation and Electron Transport Levels

Julian F. Butscher^{1,2}, Qing Sun^{1,2}, Yufeng Wu³, Fabian Stuck³, Marvin Hoffmann⁴, Andreas Dreuw⁵, Fabian Paulus^{1,2}, A. Stephen K. Hashmi^{3,5}, Nir Tessler⁶ and Yana Vaynzof^{1,2*}

¹ Kirchhoff Institute for Physics, Heidelberg University, Im Neuenheimer Feld 227, 69120 Heidelberg, Germany

² 2 Integrated Centre for Applied Physics and Photonic Materials and Centre for Advancing Electronics Dresden (cfaed), Technical University of Dresden, Nöthnitzer Straße 61, 01187 Dresden, Germany

³ Organic Chemistry Institute, Im Neuenheimer Feld 270, Heidelberg University, 69120 Heidelberg, Germany.

⁴ Interdisciplinary Center for Scientific Computing (IWR), Heidelberg University, Im Neuenheimer Feld 205A, 69120 Heidelberg

⁵ Chemistry Department, Faculty of Science, King Abdulaziz University (KAU), 21589 Jeddah (Saudi Arabia)

⁶ Sara and Moshe Zisapel Nano-Electronic Center, Department of Electrical Engineering, Technion-Israel Institute of Technology, Haifa 32000, Israel

*E-mail: yana.vaynzof@tu-dresden.de

Abstract

Herein, we report on the synthesis and investigation of two triazino-isoquinoline tetrafluoroborate electrolytes as hole-blocking layers in methylammonium triiodide perovskite photovoltaic devices with fullerene electron extraction layer. We find that increasing the thickness of the dipolar hole-blocking layer results in a gradual increase in the open-circuit voltage suggesting that aggregation of the molecules can enhance the dipole induced by the layer. This finding is confirmed by theoretical calculations demonstrating that while both molecules exhibit a similar dipole moment in their isolated state, this dipole is significantly enhanced when they aggregate. Ultra-violet photoemission spectroscopy measurements show that both derivatives exhibit a high ionisation potential of 7 eV, in agreement with their effective hole-blocking nature demonstrated by the devices. However, each of the molecules shows a different electron affinity due to the increased conjugation of one of the derivatives. While the change in electron transport level between the two derivatives is as high as 0.3 eV, the difference in the open-circuit voltage of both types of devices is negligible, suggesting that the electron transport level plays only a minor role in determining the open-circuit voltage of the device. Numerical device simulations confirm that the increase in built-in potential, arising from the high dipole of the electrolyte layer, compensates for the non-ideal energetic alignment of the charge transport levels, resulting in high VOC for a range of electron transport levels. Our study demonstrates that the application of small molecule electrolytes as hole-blocking layer in inverted architecture perovskite solar cells is a powerful tool to enhance the open-circuit voltage of the devices and provides useful guidelines for designing future generations of such compounds.

Keywords: Open-circuit voltage; Perovskite solar cells; Small molecule electrolytes; Aggregation; Device simulation.

1. Introduction

Since their discovery, perovskite solar cells (PSCs) have had an incredible journey of increasing popularity and performance, now reaching over 25 % power conversion efficiency.[1] While planar PSCs can be fabricated in two architectures, defined by the order of transport layers in the device structure, the inverted or p-i-n architecture in particular received significant attention due to its ease of fabrication[2,3] and suppressed hysteresis[4,5]. Such devices consist of a bottom hole transport layer (HTL) and a top electron transport layer (ETL) that sandwich the perovskite active layer. A range of materials have been investigated as HTLs, including inorganic oxides[6–9], polymers[10–12] or small molecules[13–15] yielding varying photovoltaic performances. Among these materials, one of the most extensively studied polymer HTL for perovskite solar cells is Poly(3,4-ethylenedioxythiophene)-poly(styrenesulfonate) (PEDOT:PSS). While this HTL is easy to process and has been applied in a range of photovoltaic devices[16–18], its low work-function, that leads to an unfavourable energy mismatch at the PEDOT:PSS/perovskite interface, significantly reduces the performance of devices employing PEDOT:PSS as HTL. In particular, the open-circuit voltage (V_{OC}) suffers as compared to devices using other higher work-function HTLs as e.g. poly[bis(4-phenyl) (2,4,6-trimethylphenyl)amine] (PTAA)[19–21] or NiO_x [22–24].

On the electron extracting side, polymers[25], or more commonly, fullerenes such as C_{60} or [6,6]-phenyl- C_{61} -butyric acid methyl ester (PCBM) are employed as it has been shown that they minimise the J-V hysteresis by trap state passivation[26]. However, the relatively low ionization potential of fullerenes as compared to the valence band of the perovskite active layer results in an undesirable hole conduction towards the cathode, causing significant loss in fill factor. To eliminate such losses, an additional layer of a material with a high ionization potential is typically added at the fullerene/cathode interface and is termed a ‘hole-blocking layer’. The positive effect on the fill factor of devices has been shown for many HBLs, including metal acetylacetonate[27], LiF[28], titanium (diisopropoxide) bis(2,4-pentanedionate)[29], and perylene-diimide[30], yet one of most commonly employed HBLs remains bathocuproine (BCP) due to its ease of fabrication and relative stability[31–33]. Most HBLs have little to no effect on the V_{OC} of the devices, especially in the case of PEDOT:PSS as a HTL. Nevertheless, we recently showed that a sufficiently large dipole moment within the BCP HBL can remove all limitations to the V_{OC} set by the lower work function of PEDOT:PSS compared to other HTLs[36]. Other approaches to overcome the unfavourable energetics of PEDOT:PSS compared to other HTLs focus on improving the properties of PEDOT:PSS by doping[18,34] and interface engineering[35].

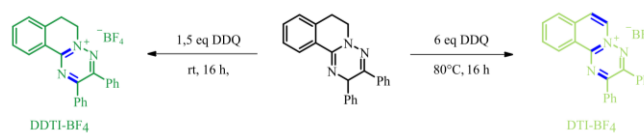
However, only few reports investigate a combined approach in which a HBL is effective in both hole-blocking and enhancing the built-in potential of the device to compensate for the unfavourable energetics on the HTL side, resulting in the simultaneous increase in both fill factor and V_{OC} [37,38].

In this work, we report on the synthesis and study of two triazino-isoquinoline tetrafluoroborate (TI- BF_4) electrolytes as HBL in inverted architecture methylammonium triiodide ($MAPbI_3$) perovskite devices. The two molecules exhibit a similarly high dipole moment that is further enhanced when the molecules are aggregated. Consequently, increasing the layer thickness results in a gradual increase in the V_{OC} of the photovoltaic devices. While both derivatives are equally effective in hole-blocking due to their high ionisation potential, the different extent of conjugation leads to very different electron transport levels. Photovoltaic performance characterisation shows that these variations are mitigated by the increase in the built-in potential of the devices, resulting in an overall very similar increase in V_{OC} . To confirm the experimental results, the effect of the different HBL electron transport levels is investigated by numerical device simulations that demonstrate that the high dipole introduced by the HBL is sufficient to compensate for both the energetic mismatch at the PEDOT:PSS interface and the variation in the electron transport level of the HBL.

2. Results and Discussion

2.1 Synthesis of Electrolytes DTI- BF_4 and DDTI- BF_4

The nitrogen scaffolds serving as starting point of the synthesis were prepared according to a previously reported procedure[39]. 1.6 eq. and 6 eq. 2,3-Dichloro-5,6-dicyano-1,4-benzoquinone (DDQ) were used for dehydrogenation, respectively. Tetrafluoroboric acid (HBF_4) was added to obtain the final 2,3-diphenyl-1-[1,2,4]triazino[3,2-a]isoquinoline-5-ium tetrafluoroborate (DTI- BF_4) and 2,3-diphenyl-6,7-dihydro-[1,2,4]triazino[3,2-a]isoquinoline-5-ium tetrafluoroborate (DDTI- BF_4) as depicted in Scheme 1. Detailed description of the synthesis procedures, as well as characterization using standard methods can be found in the Supplementary Information (Scheme S1, Figures S1-S3).



Scheme 1. Synthesis of TI- BF_4 compounds.

2.2 Effect of TI- BF_4 Aggregation on Photovoltaic Device Performance

To investigate the applicability of TI- BF_4 as hole-blocking layers in perovskite solar cells, they were incorporated in

inverted architecture solar cells with the structure: glass/ITO/PEDOT:PSS/MAPbI₃/PCBM/HBL/Ag (Figure 1a). For this purpose, devices with different HBL thicknesses, achieved by varying the concentration of the HBL solution, were fabricated and compared to reference devices with BCP as HBL. We note that the morphology of both derivatives on PCBM is very similar as evidenced by atomic force microscopy measurements (Supplementary Information, Figure S4). Figure 1b summarises the photovoltaic performance for both TI-BF₄ derivatives. As expected, the use of BCP as HBL results in a relatively low V_{OC} of only 0.96-0.98 V, in agreement with previous reports[40–42]. Replacing the BCP layer with either of the TI-BF₄ derivatives results in an increase in the V_{OC}. As the concentration of the TI-BF₄ is gradually increased from 0.25 mg/ml to 0.75 mg/ml, the V_{OC} continuously increases reaching an average of 1.05-1.07 V, and a maximum of 1.09 V. The short-circuit current and fill factor remain largely unchanged when compared to the reference BCP device resulting in an overall enhancement in device power conversion efficiency by approximately 2%. Further increase of the thickness (corresponding to a solution concentration of 1 mg/ml) is not beneficial, since especially the fill factor of the devices suffers, most likely as a result of electron transport through the layer becoming a limiting factor.

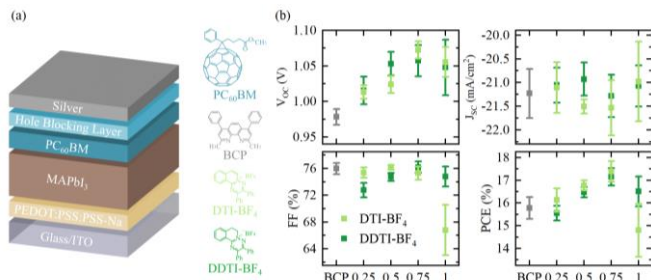


Figure 1. (a) Photovoltaic device structure with chemical structures of the materials used as extraction layers (b) Photovoltaic performance parameters of devices with increasing HBL thickness and reference BCP devices. Concentration ranges from 0.25 mg/ml to 1 mg/ml in methanol.

The increase in the V_{OC} is unlike what has been previously observed for HBLs with different thickness[37]. This increase suggests that the dipole induced by the HBLs is increasing with increasing layer thickness, which can be triggered by aggregation of the TI-BF₄ molecules. To investigate what influence aggregation may have on the dipole formed by the layer we performed theoretical calculations on either isolated molecules or on molecules in their crystalline structure. Figure 2a depicts the electron density, which was plotted (isovalue = 0.01) and colored according to a normalized gradient to highlight the differences in the electron density magnitude and the simulated dipoles of molecules DTI-BF₄ and DDTI-BF₄. Figures 2b and 2c show the Löwdin charge population analysis of the atoms in the intersecting ring perpendicular to the dipole moment in the isolated and in the

crystal structure of the molecules, respectively. In their isolated state both molecules DTI-BF₄ and DDTI-BF₄ show a similar dipole moment of 9.44 D and 9.73 D, respectively. The Löwdin charges of the atoms in the intersecting ring perpendicular to the dipole moment add to 0.083 and 0.094. As shown in Figure 2c, however, both molecules DTI-BF₄ and DDTI-BF₄ exhibit a compact aggregation behaviour leading to a considerably increased dipole-dipole interaction stemming from its inverse cubic distance dependence. Furthermore, an enhancement of the positive Löwdin charge of the two rings, intersecting the dipole moment vector, corroborates resulting polarization effects due to the compactness of the aggregation. Consequently, the total dipole moment of both aggregates is enhanced as compared to the molecules in the isolated states.

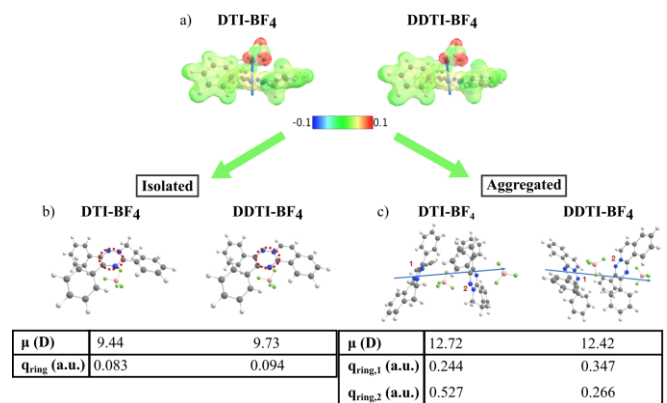


Figure 2. (a) Simulated electron density and dipole for molecules DTI-BF₄ and DDTI-BF₄. Löwdin charge population analysis of the atoms in the intersecting ring perpendicular to the dipole moment in the (b) isolated and (c) crystal structure state.

2.3 Effect of Electron Transport Levels on Photovoltaic Device Performance

To characterise the energy levels of DTI-BF₄ and DDTI-BF₄, ultra-violet photoemission spectroscopy (UPS) measurements were performed on glass/ITO/PCBM/DTI-BF₄, DDTI-BF₄ films yielding an ionization potential of 7 eV for both compounds (Figure 3a). For better comparison the weak PCBM peak still visible in the spectra of DTI-BF₄ and DDTI-BF₄ was subtracted in Figure 3a. The bandgap of both compounds in thin films was investigated using UV-vis spectroscopy (Figure 3b). Fitting the absorption onset of the spectra yields a bandgap of 2.6 eV and 2.9 eV for DTI-BF₄ and DDTI-BF₄, respectively. The complete energetic picture for both compounds as well as for PCBM and BCP is depicted in Figure 3c.

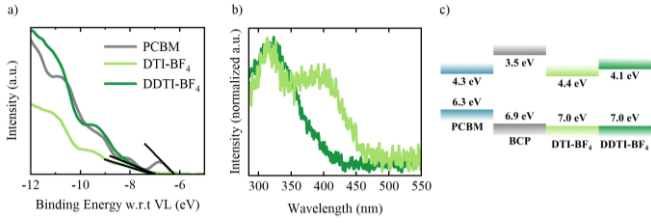


Figure 3. (a) Ultra-violet photoemission spectroscopy measurements on PCBM, DTI-BF₄ and DDTI-BF₄ the black lines indicate the ionization potentials derived from the HOMO cutoff. (b) UV-vis spectra of DTI-BF₄ and DDTI-BF₄. (c) Summary of the energy levels of BCP, DTI-BF₄ and DDTI-BF₄ HBLs with PCBM as reference.

The deep-lying highest occupied molecular orbital (HOMO) of both electrolytes suggests that their hole-blocking is equally effective as that of BCP. However, the different positions of the lowest unoccupied molecular orbital (LUMO) of the three HBLs with respect to the PCBM LUMO raises the question of the effect of the electron transport level on the performance of the solar cells. Although the LUMO of BCP lies significantly higher than the LUMO of PCBM, efficient electron transport via the BCP layer is possible due to the formation of gap states as a result of electrode evaporation.[43,44] In the case of the DTI-BF₄ and DDTI-BF₄ derivatives, their LUMOs are much deeper than that of BCP with DTI-BF₄ being slightly below and DDTI-BF₄ slightly above the LUMO of PCBM. These deviations from the PCBM LUMO may influence the device performance: for example, a lower lying LUMO may result in a lower built-in potential in the device, while alternatively a higher lying LUMO may result in an extraction barrier of electrons from the PCBM layer. To compare the photovoltaic performance of devices with both derivatives, devices with HBL layers deposited from the optimal concentration of 0.75 mg/ml were fabricated and characterised. **Figure 4a** shows the J-V curves of champion devices fabricated with either BCP or DTI-BF₄ and DDTI-BF₄ HBLs and **Table 1** summarising their photovoltaic parameters. The corresponding external quantum efficiency (EQE) spectra are shown in **Figure 4b**. Statistics acquired from 30 devices are shown in **Figure 4c**.

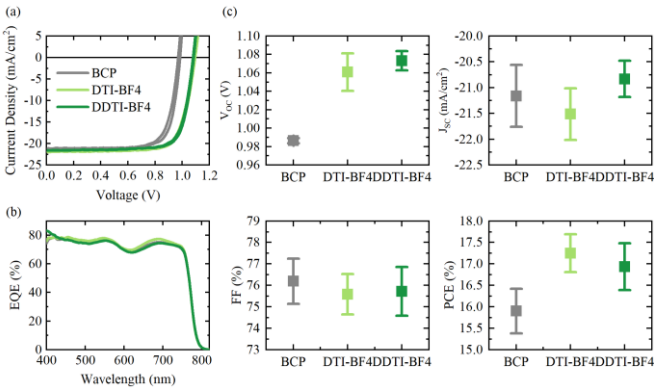


Figure 4. a) J-V-curves for champion devices with each HBL measured under one sun illumination d) External quantum efficiency spectra for each type of device. (c) Photovoltaic parameters statistics of 30 photovoltaic devices.

Despite the differences in the LUMO position between the two derivatives, they reach very similar photovoltaic performance. No significant difference in the built-in potential of the device can be observed from the dark current J-V characteristics (Supplementary Information, Figure S5), suggesting that even if variation in the electron transport level reduced the built-in potential of the device, the high dipole moment introduced by the HBL compensates for this non-ideality. Overall, with no variation in the fill factor and short-circuit current between the well-established BCP and the novel electrolyte derivatives, it is the difference in V_{OC} which determines the overall improvement in device performance. On average the V_{OC} increases by approximately 80 mV, with a maximum increase of 120 mV. Correspondingly, the maximum PCE is increased from 16.28 % for a BCP device to 18.33 % and 18.38 % for devices with DTI-BF₄ and DDTI-BF₄, respectively.

Table 1. Photovoltaic parameters of optimal MAPbI₃ devices with different hole-blocking layers. Forward Scan (from J_{SC} to V_{OC}) and Reverse scan (from V_{OC} to J_{SC}) parameters are provided.

| | Forward Scan | | | | Reverse Scan | | | |
|----------------------------|--------------|--------------------------------|--------|---------|--------------|--------------------------------|--------|---------|
| | V_{OC} [V] | J_{SC} [mA/cm ²] | FF [%] | PCE [%] | V_{OC} [V] | J_{SC} [mA/cm ²] | FF [%] | PCE [%] |
| BCP | 0.97 | -21.06 | 76.70 | 15.68 | 0.99 | -21.06 | 78.47 | 16.28 |
| DTI-BF₄ | 1.09 | -21.98 | 76.10 | 18.19 | 1.10 | -21.98 | 76.08 | 18.33 |
| DDTI-BF₄ | 1.08 | -21.57 | 77.27 | 18.00 | 1.09 | -21.57 | 78.51 | 18.38 |

To confirm that the electron transport level plays only a minor role in determining the device performance, we employed numerical device simulations in which we compare the simulated J-V characteristics of devices with HBLs with three different LUMOs. First, to simulate the case of BCP, we introduce a HBL with no dipole and an electron transport level at the same level as PCBM. Next, we compare the two electrolyte HBLs which introduce a dipole of the same strength, yet exhibiting different electron transport levels: DTI-BF₄ at 0.1 eV below and DDTI-BF₄ at 0.2 eV above the LUMO of PCBM. As a reference a HBL of the same dipole and an electron transport level equivalent to that of PCBM is also simulated (Figure S6). The results of the numerical simulations (**Figure 5**) confirm that these variations of the electron transport level have only a marginal effect on the V_{OC} with all three dipolar cases resulting in a similar V_{OC} , which is significantly higher than that of the non-dipolar HBL BCP.

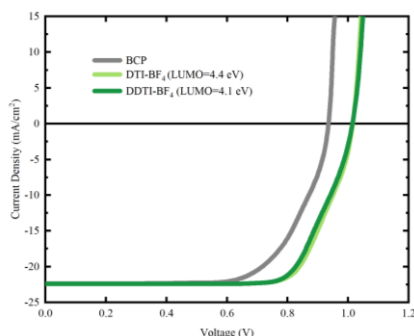


Figure 5. Simulated J-V curves of reference BCP hole-blocking layer and the two dipoles with different LUMO energies.

3. Conclusion

To summarise, we report on the synthesis and application of two novel electrolyte derivatives in inverted architecture perovskite photovoltaic devices. We demonstrate that aggregation plays an important role in determining the induced dipole and the final open-circuit voltage of the devices. We also show that while the molecules exhibit electron transport levels that vary by 0.3 eV, this variation has little to no effect on the final device performance. Our study demonstrates that dipolar HBLs are a powerful method to enhance the performance of perovskite photovoltaic devices, with particular emphasis on the importance of the dipole strength induced by the layer, rather than the position of charge transport levels.

4. Experimental Methods

Materials: Methylammonium iodide ($\text{CH}_3\text{NH}_3\text{I}$) was purchased from GreatCell Solar. PEDOT:PSS was purchased from Heraeus Deutschland GmbH&Co and PCBM (99.5%) was purchased from Solenne BV. All other materials were purchased from Sigma-Aldrich and used as received.

Photovoltaic Device Fabrication: Pre-patterned indium tin oxide (ITO) coated glass substrates (PsiOTech Ltd., 15 Ohm/sq) were subsequently cleaned in 2 % hellmanex detergent, deionized water, acetone and isopropanol in an ultra-sonicate bath. Shortly before spin coating the first layer, the samples were treated for 8 min with an oxygen plasma. PEDOT:PSS prepared based on a previous report [11] was spin coated on the substrates with 4000 rpm 30 s and annealed at 150 °C for 15 min. The samples were then transferred into a dry air filled glovebox (RH < 0.5 %). A lead acetate trihydrate MAPbI_3 recipe [45] was used for forming the MAPbI_3 perovskite layer, in detail the perovskite solution was spin coated at 2000 rpm for 60 s. After blowing 25 s with a dry air gun and resting for 5 min, the films were annealed at 100 °C for another 5 min. All samples were then transformed into a nitrogen filled glovebox where a PCBM (20 mg/ml in chlorobenzene) layer was dynamically spin coated at 2000 rpm for 30 s on the perovskite films. The films were annealed

for 10 min at 100 °C. Finally, either BCP (0.5 mg/ml in isopropanol) or the TI-BF_4 molecules (various concentrations in methanol) were dynamically spin coated at 4000 rpm for 30 s. The devices were completed with an 80 nm silver electrode that was deposited via thermal evaporation under high vacuum.

Photovoltaic Device Characterization: The current density-voltage (J-V) was measured by a computer controlled Keithley 2450 Source Measure Unit under simulated AM 1.5G sunlight with 100 mW cm^{-2} irradiation (Abet Sun 3000 Class AAA solar simulator). The light intensity was calibrated with a Si reference cell (NIST traceable, VLSI) and corrected by measuring the spectral mismatch between the solar spectrum, the spectral response of the perovskite solar cell and the reference cell. The cells were scanned from forward bias to short circuit and reverse at a rate of 0.25 V s^{-1} .

UV-vis absorption: The TI-BF_4 molecules were dissolved at 0.5 mg/ml in methanol and spin coated on clean glass substrates. The UV-Vis spectra of the resulting thin films were measured at room temperature with a Jasco UV-Vis V670 spectrometer.

Ultra-violet Photoemission Spectroscopy (UPS): Ultra-violet photoemission spectroscopy measurements were performed on PCBM/BCP and PCBM/ TI-BF_4 films to characterize their ionization potential. The samples were transferred to an ultrahigh vacuum (UHV) chamber of the PES system (Thermo Scientific ESCALAB 250Xi) for measurements. UPS measurements were carried out using a double-differentially pumped He discharge lamp ($h\nu = 21.22$ eV) with a pass energy of 2 eV and a bias of -10 V.

Dipole Simulation: Geometry optimization of the monomers were done with pbe0/pc-1 and the D3 dispersion correction within the TeraChem software package.[1,2,3] For the single point calculations the double-hybrid functional PWPB95 with the D3 dispersion correction including Becke-Johnson damping and the def2-TZVPD basis set was used as implemented in the ORCA software package.[4]

Numerical Device Simulations: A previously developed model that includes the contributions of charges and ions has been used to simulate the influence of incorporating TI-BF_4 HBL into the device structure.[46]

Acknowledgements

This work has received financial support of the Deutsche Forschungsgemeinschaft (DFG) SFB 1249 projects A03, B01 and C04. This project has also received funding from the European Research Council (ERC) under the European Union's Horizon 2020 research and innovation program (ERC Grant Agreement n° 714067, ENERGYMAPS). N.T. acknowledges support by the Israel Science Foundation (grant no. 488/16), the Adelis Foundation for renewable energy research within the framework of the Grand Technion Energy

Program (GTEP), and the Technion Ollendorff Minerva Center.

References

- [1] NREL 2019 Research Cell Efficiency Records *Natl. Renew. Energy Lab.*
- [2] Liu T, Chen K, Hu Q, Zhu R and Gong Q 2016 Inverted Perovskite Solar Cells: Progresses and Perspectives *Adv. Energy Mater.* **6** 1600457
- [3] Nie W, Tsai H, Asadpour R, Neukirch A J, Gupta G, Crochet J J, Chhowalla M, Treiak S, Alam M A and Wang H 2015 High-efficiency solution-processed perovskite solar cells with millimeter-scale grains **347** 522–6
- [4] Wu C-G, Chiang C-H, Tseng Z-L, Nazeeruddin M K, Hagfeldt A and Grätzel M 2015 High efficiency stable inverted perovskite solar cells without current hysteresis *Energy Environ. Sci.* **8** 2725–33
- [5] Tress W, Marinova N, Moehl T, Zakeeruddin S M, Nazeeruddin M K and Grätzel M 2015 Understanding the rate-dependent J-V hysteresis, slow time component, and aging in CH₃NH₃PbI₃ perovskite solar cells: The role of a compensated electric field *Energy Environ. Sci.* **8** 995–1004
- [6] Fang R, Wu S, Chen W, Liu Z, Zhang S, Chen R, Yue Y, Deng L, Cheng Y-B, Han L and Chen W 2018 [6,6]-Phenyl-C 61 -Butyric Acid Methyl Ester/Cerium Oxide Bilayer Structure as Efficient and Stable Electron Transport Layer for Inverted Perovskite Solar Cells *ACS Nano* **12** 2403–14
- [7] Song J, Zheng E, Bian J, Wang X-F, Tian W, Sanehira Y and Miyasaka T 2015 Low-temperature SnO₂-based electron selective contact for efficient and stable perovskite solar cells *J. Mater. Chem. A* **3** 10837–44
- [8] Chen W, Zhou Y, Wang L, Wu Y, Tu B, Yu B, Liu F, Tam H-W, Wang G, Djurišić A B, Huang L and He Z 2018 Molecule-Doped Nickel Oxide: Verified Charge Transfer and Planar Inverted Mixed Cation Perovskite Solar Cell *Adv. Mater.* **30** 1800515
- [9] Guo Q, Wang C, Li J, Bai Y, Wang F, Liu L, Zhang B, Hayat T, Alsaedi A and Tan Z 2018 Low-temperature solution-processed vanadium oxide as hole transport layer for efficient and stable perovskite solar cells *Phys. Chem. Chem. Phys.* **20** 21746–54
- [10] Malinkiewicz O, Yella A, Lee Y H, Espallargas G M, Graetzel M, Nazeeruddin M K and Bolink H J 2014 Perovskite solar cells employing organic charge-transport layers *Nat. Photonics* **8** 128–32
- [11] Zuo C and Ding L 2017 Modified PEDOT Layer Makes a 1.52 V Voc for Perovskite/PCBM Solar Cells *Adv. Energy Mater.* **7** 1601193
- [12] Jeon N J, Noh J H, Kim Y C, Yang W S, Ryu S and Seok S I 2014 Solvent engineering for high-performance inorganic–organic hybrid perovskite solar cells *Nat. Mater.* **13** 897–903
- [13] Song Y, Lv S, Liu X, Li X, Wang S, Wei H, Li D, Xiao Y and Meng Q 2014 Energy level tuning of TPB-based hole-transporting materials for highly efficient perovskite solar cells *Chem. Commun.* **50** 15239–42
- [14] Jeon N J, Lee H G, Kim Y C, Seo J, Noh J H, Lee J and Seok S I 2014 o-Methoxy Substituents in Spiro-OMeTAD for Efficient Inorganic–Organic Hybrid Perovskite Solar Cells *J. Am. Chem. Soc.* **136** 7837–40
- [15] Choi H, Paek S, Lim N, Lee Y H, Nazeeruddin M K and Ko J 2014 Efficient Perovskite Solar Cells with 13.63 % Efficiency Based on Planar Triphenylamine Hole Conductors *Chem. - A Eur. J.* **20** 10894–9
- [16] Tan Z K, Vaynzof Y, Credgington D, Li C, Casford M T L, Sepe A, Huettner S, Nikolka M, Paulus F, Yang L, Siringhaus H, Greenham N C and Friend R H 2014 In-situ switching from barrier-limited to ohmic anodes for efficient organic optoelectronics *Adv. Funct. Mater.* **24** 3051–8
- [17] Falk L M, Goetz K P, Lami V, An Q, Fassel P, Herkel J, Thome F, Taylor A D, Paulus F and Vaynzof Y 2019 Effect of Precursor Stoichiometry on the Performance and Stability of MAPbBr₃ Photovoltaic Devices *Energy Technol.* **1900737** ente.201900737
- [18] Huang X, Wang K, Yi C, Meng T and Gong X 2016 Efficient Perovskite Hybrid Solar Cells by Highly Electrical Conductive PEDOT:PSS Hole Transport Layer *Adv. Energy Mater.* **6** 1501773
- [19] Luo D, Yang W, Wang Z, Sadhanala A, Hu Q, Su R, Shivanna R, Trindade G F, Watts J F, Xu Z, Liu T, Chen K, Ye F, Wu P, Zhao L, Wu J, Tu Y, Zhang Y, Yang X, Zhang W, Friend R H, Gong Q, Snaith H J and Zhu R 2018 Enhanced photovoltage for inverted planar heterojunction perovskite solar cells *Science (80-.)*. **360** 1442–6
- [20] Wang Q, Bi C and Huang J 2015 Doped hole transport layer for efficiency enhancement in planar heterojunction organolead trihalide perovskite solar cells *Nano Energy* **15** 275–80
- [21] Zhao J, Zheng X, Deng Y, Li T, Shao Y, Gruverman A, Shield J and Huang J 2016 Is Cu a stable electrode material in hybrid perovskite solar cells for a 30-year lifetime? *Energy Environ. Sci.* **9** 3650–6
- [22] Zheng J, Hu L, Yun J S, Zhang M, Lau C F J, Bing J, Deng X, Ma Q, Cho Y, Fu W, Chen C, Green M A, Huang S and Ho-Baillie A W Y 2018 Solution-Processed, Silver-Doped NiO_x as Hole Transporting Layer for High-Efficiency Inverted Perovskite Solar Cells *ACS Appl. Energy Mater.* **1** 561–70
- [23] Liu Z, Chang J, Lin Z, Zhou L, Yang Z, Chen D, Zhang C, Liu S (Frank) and Hao Y 2018 High-Performance Planar Perovskite Solar Cells Using Low Temperature, Solution-Combustion-Based Nickel Oxide Hole Transporting Layer

- with Efficiency Exceeding 20% *Adv. Energy Mater.* **8** 1703432
- [24] Seo S, Park I J, Kim M, Lee S, Bae C, Jung H S, Park N-G, Kim J Y and Shin H 2016 An ultra-thin, un-doped NiO hole transporting layer of highly efficient (16.4%) organic–inorganic hybrid perovskite solar cells *Nanoscale* **8** 11403–12
- [25] Guo Q, Xu Y, Xiao B, Zhang B, Zhou E, Wang F, Bai Y, Hayat T, Alsaedi A and Tan Z 2017 Effect of Energy Alignment, Electron Mobility, and Film Morphology of Perylene Diimide Based Polymers as Electron Transport Layer on the Performance of Perovskite Solar Cells *ACS Appl. Mater. Interfaces* **9** 10983–91
- [26] Shao Y, Xiao Z, Bi C, Yuan Y and Huang J 2014 Origin and elimination of photocurrent hysteresis by fullerene passivation in CH₃NH₃PbI₃ planar heterojunction solar cells *Nat. Commun.* **5** 1–7
- [27] Chen W, Xu L, Feng X, Jie J and He Z 2017 Metal Acetylacetonate Series in Interface Engineering for Full Low-Temperature-Processed, High-Performance, and Stable Planar Perovskite Solar Cells with Conversion Efficiency over 16% on 1 cm² Scale *Adv. Mater.* **29** 1603923
- [28] Liu X, Yu H, Yan L, Dong Q, Wan Q, Zhou Y, Song B and Li Y 2015 Triple Cathode Buffer Layers Composed of PCBM, C₆₀, and LiF for High-Performance Planar Perovskite Solar Cells *ACS Appl. Mater. Interfaces* **7** 6230–7
- [29] Li C, Wang F, Xu J, Yao J, Zhang B, Zhang C, Xiao M, Dai S, Li Y and Tan Z 2015 Efficient perovskite/fullerene planar heterojunction solar cells with enhanced charge extraction and suppressed charge recombination *Nanoscale* **7** 9771–8
- [30] Min J, Zhang Z-G, Hou Y, Ramirez Quiroz C O, Przybilla T, Bronnbauer C, Guo F, Forberich K, Azimi H, Ameri T, Spiecker E, Li Y and Brabec C J 2015 Interface Engineering of Perovskite Hybrid Solar Cells with Solution-Processed Perylene–Diimide Heterojunctions toward High Performance *Chem. Mater.* **27** 227–34
- [31] Yuan D-X, Yuan X-D, Xu Q-Y, Xu M-F, Shi X-B, Wang Z-K and Liao L-S 2015 A solution-processed bathocuproine cathode interfacial layer for high-performance bromine–iodine perovskite solar cells *Phys. Chem. Chem. Phys.* **17** 26653–8
- [32] Zhou Z, Li X, Cai M, Xie F, Wu Y, Lan Z, Yang X, Qiang Y, Islam A and Han L 2017 Stable Inverted Planar Perovskite Solar Cells with Low-Temperature-Processed Hole-Transport Bilayer *Adv. Energy Mater.* **7** 1700763
- [33] Wang Q, Shao Y, Dong Q, Xiao Z, Yuan Y and Huang J 2014 Large fill-factor bilayer iodine perovskite solar cells fabricated by a low-temperature solution-process *Energy Environ. Sci.* **7** 2359–65
- [34] Liu D, Li Y, Yuan J, Hong Q, Shi G, Yuan D, Wei J, Huang C, Tang J and Fung M-K 2017 Improved performance of inverted planar perovskite solar cells with F4-TCNQ doped PEDOT:PSS hole transport layers *J. Mater. Chem. A* **5** 5701–8
- [35] Luo H, Lin X, Hou X, Pan L, Huang S and Chen X 2017 Efficient and Air-Stable Planar Perovskite Solar Cells Formed on Graphene-Oxide-Modified PEDOT:PSS Hole Transport Layer *Nano-Micro Lett.* **9** 39
- [36] Butscher J, Intorp S, Kress J, An Q, Hofstetter Y J, Hippchen N, Paulus F, Bunz U H F, Tessler N and Vaynzof Y 2019 Enhancing the Open-Circuit Voltage of Perovskite Solar Cells by Embedding Molecular Dipoles within their Hole-Blocking Layer *ACS Appl. Mater. Interfaces* **acsami.9b18757**
- [37] An Q, Sun Q, Weu A, Becker-Koch D, Paulus F, Arndt S, Stuck F, Hashmi A S K, Tessler N and Vaynzof Y 2019 Enhancing the Open-Circuit Voltage of Perovskite Solar Cells by up to 120 mV Using π -Extended Phosphoniumfluorene Electrolytes as Hole Blocking Layers *Adv. Energy Mater.* **9** 1901257
- [38] Lee J-H, Kim J, Kim G, Shin D, Jeong S Y, Lee J, Hong S, Choi J W, Lee C-L, Kim H, Yi Y and Lee K 2018 Introducing paired electric dipole layers for efficient and reproducible perovskite solar cells *Energy Environ. Sci.* **11** 1742–51
- [39] Wu Y, Tian B, Hu C, Sekine K, Rudolph M, Rominger F and Hashmi A S K 2019 Chemodivergent reaction of azomethine imines and 2 H⁻-azirines for the synthesis of nitrogen-containing scaffolds *Org. Biomol. Chem.* **17** 5505–8
- [40] Fassel P, Lami V, Bausch A, Wang Z, Klug M T, Snaith H J and Vaynzof Y 2018 Fractional deviations in precursor stoichiometry dictate the properties, performance and stability of perovskite photovoltaic devices *Energy Environ. Sci.* **11** 3380–91
- [41] Zhou P, Fang Z, Zhou W, Qiao Q, Wang M, Chen T and Yang S 2017 Nonconjugated Polymer Poly(vinylpyrrolidone) as an Efficient Interlayer Promoting Electron Transport for Perovskite Solar Cells *ACS Appl. Mater. Interfaces* **9** 32957–64
- [42] Yang L, Cai F, Yan Y, Li J, Liu D, Pearson A J and Wang T 2017 Conjugated Small Molecule for Efficient Hole Transport in High-Performance p-i-n Type Perovskite Solar Cells *Adv. Funct. Mater.* **27** 1–10
- [43] Sakurai T, Toyoshima S, Kitazume H, Masuda S, Kato H and Akimoto K 2010 Influence of gap states on electrical properties at interface between bathocuproine and various types of metals *J. Appl. Phys.* **107**
- [44] Lee J, Park S, Lee Y, Kim H, Shin D, Jeong J, Jeong K, Cho S W, Lee H and Yi Y 2016 Electron transport mechanism of bathocuproine exciton blocking layer in organic photovoltaics *Phys. Chem. Chem. Phys.* **18** 5444–52
- [45] An Q, Fassel P, Hofstetter Y J, Becker-Koch D, Bausch A, Hopkinson P E and Vaynzof Y 2017 High performance

planar perovskite solar cells by ZnO electron transport layer engineering *Nano Energy* **39** 400–8

- [46] Tessler N and Vaynzof Y 2018 Preventing Hysteresis in Perovskite Solar Cells by Undoped Charge Blocking Layers *ACS Appl. Energy Mater.* **1** 676–83